Assessment of Mycobacterium tuberculosis Pantothenate Kinase Vulnerability through Target Knockdown and Mechanistically Diverse Inhibitors

B. K. Kishore Reddy, Sudhir Landge, Sudha Ravishankar, Vikas Patil, Vikas Shinde, Subramanyam Tantry, Manoj Kale, Anandkumar Raichurkar, Sreenivasaiah Menasinakai, Naina Vinay Mudugal, Anisha Ambady, Anirban Ghosh, Ragadeepthi Tunduguru, Parvinder Kaur, Ragini Singh, Naveen Kumar, Sowmya Bharath, Aishwarya Sundaram, Jyothi Bhat, Vasan K. Sambandamurthy, Christofer Björkelid, T. Alwyn Jones, Kaveri Das, Balachandra Bandodkar, Krishnan Malolanarasimhan, Kakoli Mukherjee and Vasanthi Ramachandran

---

Updated information and services can be found at:
http://aac.asm.org/content/58/6/3312

These include:

REFERENCES

This article cites 29 articles, 13 of which can be accessed free
at: http://aac.asm.org/content/58/6/3312#ref-list-1

CONTENT ALERTS

Receive: RSS Feeds, eTOCs, free email alerts (when new
articles cite this article), more»

Assessment of *Mycobacterium tuberculosis* Pantothenate Kinase Vulnerability through Target Knockdown and Mechanistically Diverse Inhibitors

B. K. Kishore Reddy,[a] Sudhir Landge,[a] Sudha Ravishankar,[b] Vikas Patil,[a] Vikas Shinde,[a] Subramanyam Tantry,[a] Manoj Kale,[a] Anandkumar Raichurkar,[a] Sreenivasaiah Menasinakai,[a] Naina Vinay Mudugal,[b] Anisha Ambady,[b] Anirban Ghosh,[b*] Ragadeepthi Tunduguru,[b*] Parvinder Kaur,[b] Ragini Singh,[e] Naveen Kumar,[c] Sowmya Bharath,[c] Aishwarya Sundaram,[b*] Jyothi Bhat,[b] Vasan K. Sambandamurthy,[b] Christofer Björkelid,[d] T. Alwyn Jones,[d] Kaveri Das,[d] Balachandra Bandodkar,[a*] Krishnan Malolanarasimhan,[a*] Kakoli Mukherjee,[b*] Vasanthi Ramachandran[b]

Department of Chemistry, iMED infection, AstraZeneca India Pvt. Ltd., Bangalore, India[a]; Department of Bioscience, iMED infection, AstraZeneca India Pvt. Ltd., Bangalore, India[b]; Department of DMPK and Animal Sciences, iMED infection, AstraZeneca India Pvt. Ltd., Bangalore, India[c]; Department of Cell and Molecular Biology, Uppsala University, Uppsala, Sweden[d]; Cellworks Research India Pvt. Ltd., Bangalore, India[e]

Pantothenate kinase (PanK) catalyzes the phosphorylation of pantothenate, the first committed and rate-limiting step toward coenzyme A (CoA) biosynthesis. In our earlier reports, we had established that the type I isoform encoded by the *coaA* gene is an essential pantothenate kinase in *Mycobacterium tuberculosis*, and this vital information was then exploited to screen large libraries for identification of mechanistically different classes of PanK inhibitors. The present report summarizes the synthesis and expansion efforts to understand the structure-activity relationships leading to the optimization of enzyme inhibition along with antimycobacterial activity. Additionally, we report the progression of two distinct classes of inhibitors, the triazoles, which are ATP competitors, and the biaryl acetic acids, with a mixed mode of inhibition. Cocrystallization studies provided evidence of these inhibitors binding to the enzyme. This was further substantiated with the biaryl acids having MIC against the wild-type *M. tuberculosis* strain and the subsequent establishment of a target link with an upshift in MIC in a strain overexpressing PanK. On the other hand, the ATP competitors had cellular activity only in a *M. tuberculosis* knockdown strain with reduced PanK expression levels. Additionally, *in vitro* and *in vivo* survival kinetic studies performed with a *M. tuberculosis* PanK (*Mt*PanK) knockdown strain indicated that the target levels have to be significantly reduced to bring in growth inhibition. The dual approaches employed here thus established the poor vulnerability of PanK in *M. tuberculosis*.

The burden of tuberculosis (TB) has reached unprecedented levels worldwide (1), and the rapid emergence of multidrug-resistant *Mycobacterium tuberculosis* strains has now been recognized as a major challenge for global TB control measures (2). To eliminate TB as a public health problem by 2050, the incidence of infection has to fall by 16% per year for the next 30 to 40 years (3); however, the rates are falling by only 2% (1). The difficulties encountered by all efforts to address this concern have been compounded with additional impediments, including coinfection of HIV and *M. tuberculosis*, emergence and spread of multidrug-resistant (MDR) and extensively drug-resistant (XDR) *M. tuberculosis* strains, and inadequate diagnostic and control measures (2). There is an urgent need for defined TB regimens that are shorter, efficacious, and, most importantly, safer. Such therapy should be affordable and practical for use in low-resource settings and free of interactions, especially with antiretroviral regimens (4). Among the different drug exploration strategies available, the key to the success of a target-based anti-TB program rests on identification of multiple chemical scaffolds with mechanistically diverse modes of inhibition. Such a strategy could overcome some of the challenges associated with poor druggability and, possibly, the often-encountered issue of potent inhibitors lacking the ability to translate to antibacterial activity. In pursuit of identifying targets for novel antimycobacterials, it is very important to limit the choice to those targets that impact viability with the slightest perturbation in protein levels. This adverse effect on survival or persistence normally happens owing to the loss of an essential metabolite central to many vital functions. The current report presents an evaluation of the use of one of the key enzymes of the coenzyme A (CoA) biosynthetic pathway as an option for designing a new anti-TB drug. The CoA cofactor is an essential acyl group carrier indispensable for respiration and lipid metabolism in various organisms. Loss of intracellular CoA levels either through the use of inhibitors or gene knockouts of the enzymes involved in the biosynthetic pathway have demonstrated that inhibition of CoA syn-

TABLE 1 Bacterial strains and plasmids used in this study

Strain or plasmid	Description[a]	Source or reference
Strains		
E. coli pMOS Blue	F′ *endA1* hsdR17 (r_K^- m_K^+), *supE44 thi-1 recA1 gyrA96 relA1 lac* [F′ *lac*IᵠZΔM15 *proAB*⁺ *Tn*10 (Tetʳ)]	GE Healthcare
M. tuberculosis H37Rv ATCC 27294	Virulent laboratory strain of *M. tuberculosis*	AZI collection
M. bovis BCG—CoaA OE strain	*Mt*PanK-overexpressing *M. bovis* BCG	This study
Plasmids		
pBAN0477	*M. tuberculosis coaA* gene cloned at NdeI and BamHI cloning site, Hygʳ	This study
pAZI9018b	*E. coli*-mycobacterial IPTG-inducible shuttle vector—a replicating vector with *lacZ*, Hygʳ, NdeI, and BamHI as cloning sites	12
pBAN0317	*M. tuberculosis coaA* conditional expression vector with truncated, mutant *coaA* gene cloned downstream of pristinamycin-inducible promoter (pPTR)	This study
pAZI9479	Mycobacterial conditional-expression (integrating) vector with pPTR system	13

[a] Tetʳ, tetracycline resistance; Hyg, hygromycin resistance.

thesis is a viable option to discover new antimicrobials (5–7). Significant differences between the bacterial and human counterparts enable selective inhibition of the targets on this pathway. However, for slow-growing pathogens such as *M. tuberculosis*, which are known to persist within the host for extended periods, there is an added requirement of complete killing of the pathogen and its elimination from the host to ensure a cure.

CoA is assembled in five steps from pantothenate, and the first reaction in this pathway, the phosphorylation of pantothenate to yield 4′-phoshopantothenate, is catalyzed by the enzyme pantothenate kinase (PanK). PanK, the key rate-determining enzyme of the CoA biosynthesis pathway (8), exists in three different isoforms. Type I PanK, encoded by the *coaA* gene, is present in many bacterial species, including *Escherichia coli*. Type II PanK is found mostly in eukaryotes but also in some bacteria, including *Staphylococcus aureus*. Other bacteria, such as *Bacillus anthracis*, utilize a type III PanK, encoded by the gene *coaX*. Recent work with a conditional *coaX* mutant has demonstrated that *B. anthracis* type III PanK is an essential enzyme, thereby validating this enzyme as an antimicrobial target (30). The same conclusion could not be extended to and established for the *M. tuberculosis coaX* gene, since a deletion mutant showed no growth defects *in vitro*, in macrophages or in mice, thereby ruling out the essentiality of *coaX* in this organism (9). In contrast, *coaA* could be inactivated only in the presence of an extra copy of the gene, thus proving its essentiality for the survival of *M. tuberculosis* (9).

We had earlier reported the identification of *M. tuberculosis* PanK (*Mt*PanK) inhibitors with multiple modes of inhibition obtained through screening of large libraries (10), an approach that could pave the path for evaluating targets such as *Mt*PanK. Among these, the triazoles were found to be competitive with ATP, while the biaryl acids were mixed noncompetitive. Specific interaction with the target was shown by determining the crystal structures with both types of inhibitors bound in the enzyme (11). These inhibitors were then evaluated for their ability to translate to cellular growth inhibition with *in silico* predictive tools as well as *in vitro* experimentation. In order to confirm the link with the target for compounds that had cellular activity, MIC modulation studies were carried out with *Mt*PanK overexpression and knockdown strains. However, the lack of cellular inhibition with some of the inhibitors prompted us to investigate this further through a two-pronged strategy: (i) exploration of chemical space to get more

inhibitors with nanomolar enzyme potency and (ii) assessment of vulnerability by conditional expression of *Mt*PanK.

MATERIALS AND METHODS

Bacterial strains, media, chemicals, and reagents. *E. coli* MOS Blue cells (Amersham) were used for gene cloning and plasmid propagation. The *M. bovis* BCG-Pasteur Merieux wild-type strain and *M. smegmatis* mc²155 were used as expression hosts. *M. tuberculosis* H37Rv ATCC 27294 was used to generate a *coaA* conditional-expression strain. Electrocompetent *E. coli* and mycobacterial cells were prepared as described earlier (12). All the enzymes used for cloning were from either New England BioLabs or GE Healthcare. Isopropyl-beta-thiogalactopyranoside (IPTG), rifampin, and isoniazid were obtained from Sigma, hygromycin was from Roche, and pristinamycin (Synercid) was from Sanofi Aventis. Zirconia beads (0.1 mm diameter) and a Mini-BeadBeater were purchased from Biospec Products. In general, LB medium was used for *E. coli* growth and 7H9 medium (Middlebrook 7H9 medium supplemented with 1% albumin-dextrose-catalase [ADC], 0.2% glycerol, and 0.05% Tween 80) for mycobacterial growth. Unless otherwise mentioned, the *coaA* conditional-expression strain was grown in 7H9 medium supplemented with 50 μg/ml hygromycin and 10 ng/ml pristinamycin 1 (P₁). Details of the strains used in this study are summarized in Table 1.

Protein expression, purification, and inhibitor screening for IC₅₀ determinations in *Mt*PanK assay. *Mt*PanK expression, purification, and activity assays were carried out as described earlier (10). Routine screening and 50% inhibitory concentration (IC₅₀) estimations for the *Mt*PanK inhibitors were carried out by keeping both substrate and cofactor concentrations at their respective K_m values, i.e., pantothenate at 122 μM and ATP at 395 μM. For selected inhibitors, competition with ATP was checked by measuring IC₅₀ at a 50× K_m ATP concentration, i.e., 6 mM.

Generation of recombinant *M. bovis* BCG overexpressing *Mt*PanK. The full-length *coaA* gene was PCR amplified from *M. tuberculosis* genomic DNA using primers MtbcoaAF (5′-ATTCCAACATATGATGTCGCGGCTTAGCGAGCC-3′) and MtbcoaAR (5′AGGCCTAGGATCCTTACAGCTTGCGCAGCCGCA-3′). Recombinant plasmid pBAN0477 was generated by cloning the amplicon at BamHI and NdeI sites of pAZI9018b, a replicating *E. coli*-mycobacterium shuttle vector, with an IPTG-inducible promoter (12). Following transformation into *M. bovis* BCG, recombinants were identified by PCR and the transcript levels were monitored by reverse transcription-PCR (RT-PCR).

MIC tests were set up per CLSI (Clinical and Laboratory Standards Institute) guidelines (14). Modes of action of the triazoles and the biaryls were evaluated by MIC modulation using a *M. tuberculosis coaA* knockdown strain (*coaA*KD) (described below) and a BCG strain overexpressing *Mt*PanK, respectively. Wild-type *M. tuberculosis* and *M. bovis* BCG were used as control strains. Isoniazid and rifampin served as refer-

ence drugs. MICs were determined in the presence of 100 μM IPTG for the *Mt*PanK overexpression strain and either 0 or 10 ng/ml P₁ for the *M. tuberculosis coaA*KD strain. These MIC tests were performed in 96-well plates using the Microplate alamar blue method (15) for a 7-day measurement and the turbidometric method for a 14-day measurement.

Generation of *M. tuberculosis coaA*KD. pAZI9479 is a conditional-expression vector (13) derived from the pAZI9018b replicating plasmid. Removal of the mycobacterial origin of replication and replacement of the IPTG-inducible promoter system with a pristinamycin-inducible promoter system (unpublished data) yielded pAZI9479. This integrating vector is particularly useful for generating single-crossover knockdown strains through homologous recombination. *M. tuberculosis coaA* conditional-expression vector pBAN0317 was generated by cloning a truncated synthetic gene of *coaA* (bp 1 to 798) carrying an in-frame stop codon at codon 117 into pAZI9479 at NcoI-SphI sites. Transformants were selected on 7H10 plates supplemented with 50 μg/ml hygromycin and 100 ng/ml of P₁. A set of PCRs was performed to confirm the genotype of the recombinant *coaA* conditional-expression strain. The minimum inducer required for the growth of this strain was determined by plating dilutions of this culture on 7H10 plates supplemented with 0 to 100 ng/ml of P₁.

***In vitro* growth kinetics of the *M. tuberculosis coaA*KD strain.** A culture of the *M. tuberculosis coaA*KD strain was grown in 7H9 broth supplemented with 50 μg/ml hygromycin and 10 ng/ml P₁ up to the mid-log phase. Harvested cells were washed three times with plain 7H9 medium, resuspended in fresh medium, and used as an inoculum for both *in vitro* growth kinetics and *in vivo* phenotyping experiments. In brief, the culture concentrate was used as a master stock to inoculate 7H9 broth supplemented with 50 μg/ml hygromycin to get an optical density at A_{600} of ~0.01. This master culture was further split into 3 parts and supplemented with 0, 10, and 25 ng/ml of P₁. The growth kinetics of these cultures were monitored by measuring A_{600} and enumerating CFU at regular intervals. At each time point, dilutions of these cultures were assessed for CFU on 7H10 agar plates without (for revertants) and with (for survivors) 10 ng/ml of P₁.

Measurement of intracellular PanK levels by Western blotting. Cultures (10 ml) of wild-type *M. tuberculosis* H37Rv and *M. tuberculosis coaA*KD strains were harvested 6 days post-P₁ treatments. The cell pellets were washed twice in phosphate-buffered saline (PBS) and resuspended in about 500 μl of PBS supplemented with a cocktail of protease inhibitors. Cell suspensions were transferred to 2-ml screw-cap tubes (Biospec Products) containing about 0.1 g of 0.1-mm-diameter Zirconia beads (Biospec Products). Cell lysates were prepared by bead beating the cell suspension twice at 4,000 × *g* for 20 s each time. Protein estimation using Bradford reagent was performed on the clarified lysates obtained after centrifuging the cell lysates at 12,000 × *g* for 5 min. Two micrograms of total protein of each sample was analyzed by SDS-PAGE, after which the proteins were blotted onto a Hybond nitrocellulose membrane (GE Healthcare). Rabbit polyclonal anti-PanK serum (diluted 1:400,000) was used for probing the blot and developed using an ECL kit (GE Healthcare). Densitometric analysis of the bands on the autoradiogram was done using the Quantity One tool on the Bio-Rad gel documentation system.

***In vivo* phenotyping.** The AstraZeneca Animal Ethics Committee, registered with the government of India (registration no. CPCSEA 99/5), approved all animal experimental protocols and usage. The culture stocks were prepared as described above. BALB/c mice (8 to 10 weeks old) were infected with about 10⁶ CFU of either the *M. tuberculosis* H37Rv strain or the *M. tuberculosis coaA*KD strain. Three mice per group per time point were sacrificed at designated days postinfection to monitor the course of infection. Lung and spleen homogenates from these infected animals were tested for viable bacteria on 7H10 plates for wild-type *M. tuberculosis* H37Rv and on 7H10 agar plates supplemented with 50 μg/ml hygromycin and 50 ng/ml of P₁ for *M. tuberculosis coaA*KD.

Prediction of the most ideal type of PanK inhibition using simula-

tion. A virtual platform was built for mapping a network of pathways of *M. tuberculosis* with Cellworks' proprietary technology (iC-PHYS) using ordinary differential equations along lines similar to those used for *E. coli* experiments (16). In this mathematical model, more than 10 key pathways (glycolysis, tricarboxylic acid [TCA], pentose phosphate, glyoxylate shunt, branched-chain amino acid synthesis, and mycolic acid biosynthesis and other cell wall component biosynthetic pathways, including arabinogalactan, peptidoglycan, PIM-LAM, etc.) were simulated. Additionally, this platform could predict the outcome of any type of inhibitor-target interaction (competitive, noncompetitive, mixed mode, and uncompetitive) as well as the resultant modulation in metabolite levels within the cells. This *in silico* kinetic platform is also equipped to evaluate and differentiate between genetic and chemical vulnerability. In the case of the genetic vulnerability assessment, the target level is sequentially reduced and the impact on cell viability monitored, whereas in the case of the chemical vulnerability assessment, cell viability is evaluated by incorporating the kinetic parameters (rate constants, K_m, V_{max}) of the target as well as its substrate and products into the platform. In both cases, biomass levels served as indicators of cell growth. The inhibitors were ranked with respect to their $[I]/K_i$ values so as to gauge the lowest MIC for each type of inhibition (16). The K_i value used for this simulation was 0.1 μM.

Chemical synthesis. (i) Triazoles. Triazoles were synthesized starting with coupling of thiosemicarbazide 1 with N-BOC (N-butoxycarbonyl) amino acid 2 in the presence of HATU {1-[*bis*(dimethylamino)methylene]-1*H*-1,2,3-triazolo[4,5-b]pyridinium 3-oxid hexafluorophosphate} to get corresponding amide 3, which underwent cyclization in the presence of sodium hydroxide to afford triazole 4. The free thiol group of 4 was alkylated with halide 5 to give triazole 6, which, upon deprotection followed by coupling with acid chloride, gave triazole 7 (Fig. 1). Diversity in the scaffold was introduced by thiosemicarbazides 1 or amino acids 2 or alkyl halides 5 and acid chlorides.

(ii) Quinolones. Quinolone ureas were synthesized starting from substituted anilines as given in Fig. 2. Acetylation of substituted aniline 8 resulted in corresponding acetanilide 9, which under Vilsmeier-Haack reaction conditions afforded chloroquinoline aldehyde 10. Aldehyde 10 was converted into quinolone aldehyde 11 using sodium acetate and acetic acid. Compound 11, upon reductive amination with various amines 12, afforded secondary amines 13, which on reaction with isocyanates 14 afforded ureas 15.

(iii) BAA. Biaryl acetic acids (BAA) were synthesized starting from 3-hydroxy benzaldehyde as given in Fig. 3. Bromination of benzaldehyde 16 at 0°C resulted in 2-bromo-5-hydroxybenzaldehyde 17. Reductive alkylation of benzaldehyde 17 with piperazine 18 gave intermediate 19, which, upon subsequent arylation with various boronic acids following the Suzuki coupling protocol, led to benzaldehyde 20. Alkylation of benzaldehyde 20 with alkyl bromoacetates using Na₂CO₃-dimethylformamide (DMF) resulted in compounds 21 to 23, which, upon subsequent hydrolysis, afforded the desired biaryl acetic acids 24 in good yields. Biaryl acetamides 25 were synthesized starting from biaryl acetic acids 24 using the HATU/DIEA (diisopropylethylamine) protocol.

RESULTS

Identification of diverse chemical series targeting *Mt*PanK. We conducted two high-throughput screening (HTS) campaigns for identification of inhibitors of the *Mt*PanK enzyme. The first effort (campaign 1) screened a diverse library of ~70,000 compounds, while the second effort (campaign 2) screened a larger library of ~1,000,000 compounds. Campaign 1 chemistry focused on triazole and quinolone scaffolds which were shown to be competitive inhibitors of ATP. In order to increase the diversity of the inhibitor classes, series which were prioritized from campaign 2 were either uncompetitive with ATP (thiazole) or mixed noncompetitive with ATP (biaryl acetic acid and quinoline carboxamide). The
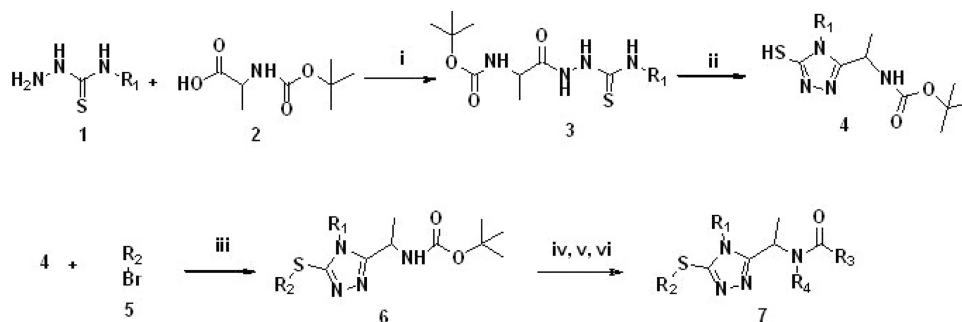
FIG 1 Synthesis of triazoles. Reagents and conditions were as follows: i, HATU, DIEA, dichloromethane (DCM), room temperature, 12 h, 60% to 70%; ii, 15% aqueous NaOH, MeOH:1,4 dioxane (1:1), room temperature, 3 h, 60% to 70%; iii, K_2CO_3, tetrahydrofuran (THF), 40°C, 16 h, 80% to 90%; iv, trifluoroethanoic acid (TFA), DCM, 0°C to room temperature, 3 h, 90%; v, ArCoCl, triethylamine (TEA), DCM, 0°C to room temperature, 2 to 3 h, 40% to 50%; vi, MeI, NaH, THF, 0°C to room temperature, 40%.

kinetic mechanism of each scaffold was characterized in detail as described earlier (10). The detailed mode of binding of a subset of triazole and biaryl acid inhibitors was determined by crystallographic studies on enzyme-inhibitor complexes. These inhibitors were found to occupy overlapping positions with CoA and each other (11).

SAR for triazoles and quinolone ureas. The two series, namely, triazoles and quinolones, were identified as hits from a 70K library screening. Both the series had a molecular mass of about 430 Da and multiple handles to develop the structure-activity relationship (SAR). Inhibitors from both series were primarily competitive with ATP. The initial IC_50 values of representatives of both series were about 100 nM at K_m ATP, and the potency was reduced by 3.5- to >100-fold when the ATP concentration was increased to $50\times K_m$ ATP. The SAR of the two series is described in detail below.

Triazoles. The SAR for the triazole series is summarized in Table 2. Compound 7m was the initial hit in this series, with an IC_50 of 87 nM at K_m ATP which then increased to 5.5 μM at $50\times K_m$ ATP. All subsequent optimization was done by following the IC_50 at $50\times K_m$ ATP. Substitution on the R2 ring to *p*-chloro (7l) and *o*-methyl (7k) groups resulted in potencies of 3.1 and 2.8 μM, respectively. When the R1 group on triazole nitrogen was changed to N-4-fluorobenzyl (7i), potency improved to 0.7 μM and further improved to 0.32 μM upon N-methylation of the amide (7h).

With a 3-pyridyl methyl substitution at triazole nitrogen, R1 was found to be the best in terms of potency (Table 2). The order of potency for N substitutions was N-3-pyridyl meth-yl→N-benzyl→N-Me. Replacement of the trifluoro methyl group (7d) on the R3 phenyl ring with chloro (7j) reduced the enzyme potency to 0.9 μM from 0.2 μM. Introduction of a second substitution in the ring brought back the potency; thus, 7c showed an IC_50 of 0.19 μM. The most potent molecule, 7a, with an IC_50 of 0.08 μM at $50\times K_m$ ATP, was obtained when the 4-fluoro benzyl group replaced the three-atom linker on the left side of triazole.

Quinolones. Compound 15d (Table 3) was one of the early hits, with an IC_50 of 1.6 μM at $50\times K_m$ ATP. Substitution on the R3 ring with 2-fluoro (15f) resulted in a loss of activity. The substitution requirement was exactly opposite in the case of the chloro group on the ring. The compound (15g) with a 4-chloro group was inactive, while the 2-chloro derivative (15c, with IC_50 = 0.5 μM) was three times more potent than 15d. The 15e compound that had a methoxy group replaced by a fluorine had activity comparable to that of 15d. Regarding substitutions on the tertiary nitrogen of the urea, the cyclopropyl substitution (15h) was inactive. When a cyclohexyl group of 15d was changed to cycloheptyl, the 15a compound showed the best IC_50 at 0.2 μM. On the other hand, the difluoro derivative (15b) showed a slight loss in potency (IC_50 at 0.6 μM). When the cycloalkyl groups were changed to aryl or heteroaryl, loss of activity was observed (data not shown).

Triazoles and quinolones were screened for MICs against wild-type *M. tuberculosis* along with the *M. tuberculosis coaA*KD strain in the absence and presence of 10 ng/ml P_1. The wild-type and *M. tuberculosis coaA*KD strains did not show any growth inhibition in the presence of 10 ng/ml P_1, while MICs were observed under
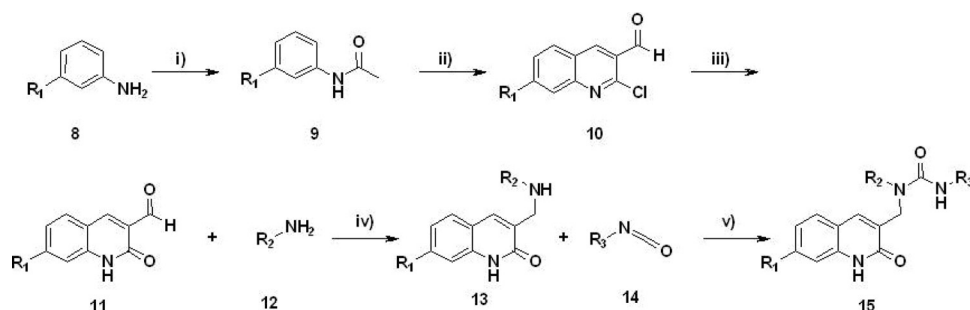

FIG 2 Synthesis of quinolone ureas. Reagents and conditions were as follows: i, AcCl, TEA, DCM, 0 to 25°C, 3 h, 99%; ii, POCl_3, DMF, 0 to 80°C, 16 h, 80%; iii, NaOAc·3H_2O, AcOH, 110°C, 3 h, 80%; iv, NaCNBH_3, AcOH, 2-propanol, 40°C, 1 h, 50% to 60%; v, DMAP (4-dimethylaminopyridine), DCM, 2 h, 40% to 50%.
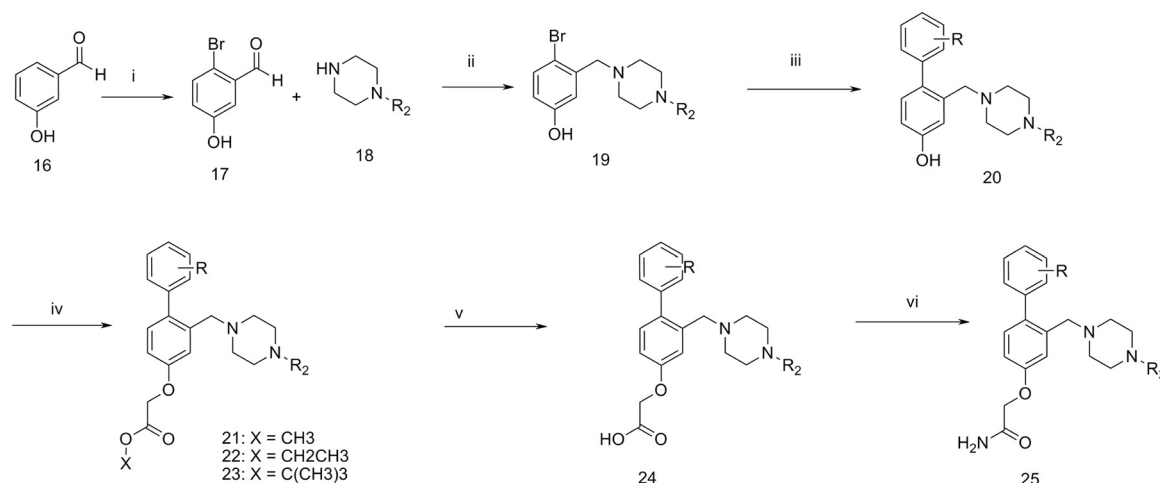
FIG 3 Synthesis of biaryl acetic acids. Reagents and conditions were as follows: i, Br_2, DCM, 0 to 2°C, 17 h, 76%; ii, $NaCNBH_3$, MeOH, room temperature, 2 h, 68%; iii, boronic acids, $Pd(PPh_3)_4$, dimethyl ether (DME):1 M Na_2CO_3 (2:1), reflux, 5 h, 60%; iv, alkyl bromoacetate, K_2CO_3, acetone, 70%; v, 5 N HCl:CH_3CN (1:3), 70% to 90%; vi, HATU, DIEA, aq. NH_3, 80%.

knockdown conditions (without P_1) for a few compounds, indicating specific target engagement. The improvement in 14-day MIC values over the 7-day values suggested a requirement for longer incubation period so as to allow sufficient inhibition of the target and, consequently, arrest of cell growth. Isoniazid, the known anti-TB drug, served as a negative control in these experiments (Table 4).

Biaryl acetic acids. Initial hits from the biaryl acetic acid series (see the representative structure in Fig. 4) were weak inhibitors of the enzyme (IC_{50} of ~8 to 10 μM); hence, several analogs were synthesized to improve the potency. In order to track the SAR, three major modifications were made.

(i) Substitutions at the aryl position of the biphenyl ring. In a traditional medicinal chemistry approach, the phenyl ring was replaced with electron-withdrawing groups (EWG) or electron-donating groups (EDG) or replaced with heteroaryl groups. The SAR data of biraryl acids (Table 5) suggested that the 4′ position is the preferred position for substitutions improving enzyme potency and, notably, that EWG members were preferred to EDG members. Further, a model experiment with a chlorosubstitution at the *ortho-*, *meta-*, and *para-* position indicated that the *para-* substituent was approximately 15-fold more potent than its *ortho-* and *meta-* counterparts (24b to 24d). The trend was similar with other EWG members (24i, 24j, 24l, and 24n). We explored the possibility of replacing the aryl with heteroaryl rings such as pyridine (24g to 24h). The position of an aza group on the heteroaryl did not have any bearing on enzyme potency. However, introducing a cyano group at the 4′ position of pyridine (24k) brought back potency. It is certain that the EWG members have a critical role to play in enhancing the enzyme potency.

(ii) The aryl piperazine substitutions. An attempt to add chirality by introducing a methyl group on the methylene between the biaryl and the piperazine rings (24t) did not provide improvements in potency. It was observed that the optimal potency could be achieved with the 2′-pyridyl piperazines (24j). Any deviations made by either changing the aza position to 4′-pyridyl piperazine or substituting pyridyl with other aryl groups proved to be detrimental to enzyme inhibition (24r and 24s). In addition, enzyme

potency was lost when the aryl ring was moved farther away by converting it into either a benzylic or an amidic linker (data not shown).

(iii) Oxyacetic acid at the 4′ position. It is clear from Table 5 that although the carboxylic acids had very good enzyme inhibition, it did not translate to potent antimycobacterial activity. This could be attributed to the lower level of permeation of biaryl acetic acids across the mycobacterial cell membrane. In order to find a suitable replacement for acids, we synthesized its bioisostere— tetrazole (26). This compound was as potent as the parent acid in terms of enzyme potency; however, this too did not translate into cellular potency, with the MIC remaining at 64 μg/ml (Table 6).

Esters are known to act as prodrugs for acids, as they get hydrolyzed by various esterases inside the bacterial cell. Keeping this in mind, we synthesized methyl and ethyl esters (Table 6, 21a and 22a) of the parent compound (Table 5, 24j). We observed that these esters have cellular potency with MICs ranging from 4 to 64 μg/ml in addition to retaining a reasonable potency on the enzyme. Ethyl ester 22b (Table 6) was a weak inhibitor of the enzyme with an IC_{50} of 50 μM; however, for the same compound, the cellular potency remained at 4 μg/ml. This clearly indicated that the enzyme potency of the acids correlated well with the cellular potency of the esters. Similar trends were observed with compounds 21b and 21d (Table 6). Compound 23a (Table 6) was screened against *M. bovis* BCG strains with overexpressed PanK. MIC values in wild-type *M. tuberculosis* H37Rv and in *M. bovis* BCG were similar, whereas the BCG strain with increased PanK levels clearly showed higher MIC values (>64 μg/ml), thus linking cellular potency to inhibition of the target enzyme.

Crystallographic studies. Crystal structures of protein-inhibitor complexes of *Mt*PanK with triazole and biaryl classes of compounds have previously been described (11). The typical binding modes of the triazole and biaryl compounds are exemplified by compound 7i (PDB identification no. [ID] 4BFW) in Fig. 5A and compound 24j (PDB ID 4BFY) in Fig. 5B, respectively. Despite differences in the mode of inhibition, compounds of the two

TABLE 2 SAR of triazoles

Entry	Compound R2	R1	R3	R4	IC$_{50}$ (μM)	Median IC$_{50}$ (μM) At 50× K_m ATP	MIC (μg/ml)
7a	4-fluorobenzyl	pyridyl	chloro-fluorophenyl	H	<0.006	0.08	>64
7b	4-fluorobenzyl	pyridyl	CF$_3$-phenyl	H	<0.006	0.18	>64
7c	4-fluorophenoxy	pyridyl	chloro-fluorophenyl	H	<0.024	0.19	>64
7d	4-fluorophenoxy	pyridyl	CF$_3$-phenyl	H	0.013	0.2	>32
7e	4-fluorobenzyl	fluorobenzyl	CF$_3$-phenyl	CH3	0.013	0.23	>32
7f	4-fluorophenoxy	pyridyl	CF$_3$-phenyl	CH3	0.012	0.24	>64
7g	4-fluorobenzyl	pyridyl	difluorophenyl	H	<0.024	0.28	>64
7h	4-fluorophenoxy	fluorobenzyl	CF$_3$-phenyl	CH3	0.023	0.32	>32
7i	4-fluorophenoxy	fluorobenzyl	CF$_3$-phenyl	H	0.054	0.7	>32
7j	4-fluorophenoxy	pyridyl	chlorophenyl	H	0.037	0.90	>64
7k	2-methylphenoxy	CH3	CF$_3$-phenyl	H	0.142	2.8	>32
7l	4-chlorophenoxy	CH3	CF$_3$-phenyl	H	<0.092	3.1	>32
7m	4-fluorophenoxy	CH3	CF$_3$-phenyl	H	0.087	5.5	>64

classes share a binding site which overlaps that of pantothenate and CoA (Fig. 5C).

Binding mode of the triazole compounds. Members of the triazole class of compounds form a U-shaped conformation similar to the shape of CoA, where the substituted phenyl rings are roughly coplanar (Fig. 5C). One of the two nitrogens in the triazole ring forms a hydrogen bond (HB) with the hydroxyl group of Tyr235, whereas the other makes a HB with the amide side chain of Asn277. The carbonyl group of the amide linker makes a HB with a water molecule, and the trifluromethyl at the ortho position of phenyl ring is in close proximity to His179. No HB interactions were observed for the oxygen in the thioether side chain, and this could explain the retention of activity with compounds lacking oxygen in the thioether side chain (7a, 7b, 7e, and 7g). The 4-fluoro phenyl ring attached to the thioether linker binds in a hydrophobic pocket composed of the side chains of Val199, Ala100, Tyr235, Phe239, and Met242. The ring is also parallel to the plane of the guanidinium group of Arg238, with the fluorine atom above the plane (11).

We have not been able to cocrystallize the inhibitor-PanK complex with ATP or ATP analogues. Therefore, we have compared our enzyme-inhibitor complexes with the *E. coli* PanK (*Ec*PanK) structure in complex with the ATP analogue AMPPNP (17) to help evaluate the effect of ATP on enzyme-inhibitor interactions. The loss of potency in the presence of ATP (Table 2) correlates with potential contacts of the R3 halogen substitution with the gamma-phosphate of the ATP analogue (11). In our modeling, 7m (the inhibitor showing the largest drop in potency) has a fluorine-phosphate oxygen contact of 2.3 Å, while for 7i (the least-affected triazole for which we have an enzyme-inhibitor complex), the closest contact is increased to 3.2 Å. Note that the difference between 7i and 7m is the R1 substitution (a large fluor-benzyl-to-methyl change discussed in more detail below) and is accommodated but results in small conformational changes in the active site that affect the detailed set of interactions between the inhibitor and enzyme. Removing the *ortho* substitution at R3 is likely to result in a loss of potency in the absence of ATP but may increase potency at higher ATP levels.

The structure of the enzyme-7i complex illustrates how substitutions are accommodated at R1. The fluor-benzyl group fits into a preformed tunnel into the active site that is not involved in the binding of substrates or CoA. The tunnel surface is mostly hydrophobic and lined by side chains from four segments of the protein, including Tyr182, Phe254, Tyr257, Ile272, and Ile276. The structure suggests that the increased potency of N-3-pyridyl methyl substitutions arises from a hydrogen bond interaction to the hydroxyl group of Tyr257.

Three pairs of compounds (compounds 7a and 7c, compounds 7b and 7d, and compounds 7e and 7h) demonstrated the effect of modifying the length of the R2 group. In all cases, the short-chain 4-fluoro thiobenzyl variant was the most potent. Most of our enzyme-inhibitor complexes had been determined with long-chain variants. However, we had one complex where the inhibitor was a 4-fluoro benzyl variant of 7m. In this complex, the side chain of Tyr182 had a different rotamer conformation, bringing it closer to the 4-fluoro thiobenzyl group. The increased potency associated with the 4-fluoro thiobenzyl variants was presumably a consequence of these changes.

Binding mode of biaryl class. The mode of binding of the biaryl class of compounds is exemplified by the crystal structures

TABLE 3 SAR of quinolone amide

Entry	Compound			IC_{50} (μM)	Median IC_{50} (μM) At 50× K_m ATP	MIC (μg/ml)
	R3	R2	R1			
15a	4-F-phenyl	cycloheptyl	O-ether	0.18	0.21	>64
15b	2,4-diF-phenyl	cycloheptyl	O-ether	<0.05	0.6	>64
15c	2-Cl-phenyl	cyclohexyl	O-ether	0.5	0.5	>64
15d	4-F-phenyl	cyclohexyl	O-ether	0.5	1.6	>64
15e	4-F-phenyl	cyclohexyl	F-alkyl	0.20	3.2	>64
15f	2-F-phenyl	cyclohexyl	O-ether	0.15	>25	>64
15g	4-Cl-phenyl	cyclohexyl	O-ether	0.25	>25	>64
15h	4-F-phenyl	cyclopropyl	O-ether	>50	>25	>64

in complex with 24j and 25b (PDB ID 4BFY and 4BFZ), representing acid and amide functionality, respectively, at the ether linkage (Fig. 5B). Except for these changes, the enzyme-inhibitor interactions are very similar. The para-nitrile phenyl group occupies the hydrophobic tunnel formed by different segments of the enzyme. One face of the ring packs against the side chain of residue Ile276, while the other has no interactions with the surface residues of the tunnel and would be exposed to solvent in the molecular dimer. The para-nitrile group is located 3.2 Å above the peptide plane connecting Met144 and His145. Whether these interactions are sufficient to explain the increased potency of 24j relative to 24a requires more-detailed computational analysis. In the crystal, however, we have a PanK dimer in the asymmetric unit that combines with a crystallographic 2-fold axis to create an assembly with 222 symmetry. Within this assembly, the para-nitrile phenyl

group interacts with the guanidinium group of Arg274 from a 2-fold related dimer. However, we have no evidence that the assembly we observed in the crystal is also relevant in solution. The reduced potencies of *ortho-* and *meta-* substitutions are equally difficult to explain. The increase in potency observed by the introduction of a methyl group at the *ortho* position (24o) indicates an interaction with a side chain of Ile272.

The lack of potency as a result of introducing a methyl group on the methylene between the biaryl and the piperazine rings (24t) arises due to potential close contacts to the side chains of Ile272 and Ile276. One of the nitrogens of the piperazine ring makes water-mediated HBs with side chains of Tyr235 and Asn277, whereas the oxygen of the ether linkage makes a HB with the hydroxyl of Tyr182. The nitrogen of the pyridine ring makes a hydrogen bond to a water molecule. The introduction of a methyl

TABLE 4 MIC modulation studies with the *coaA*KD strain

| Compound ID | *Mt*PanK IC$_{50}$ (50× K_m ATP) (μM) | MIC (μg/ml)^a | | | | | |
| | | *M. tuberculosis* H37Rv | | *coaA*KD with 10 ng/ml P$_1$ | | *coaA*KD without P$_1$ | |
		D7	D14	D7	D14	D7	D14
7a	0.08	>64	>64	>64	>64	16	16
7b	0.18	>64	>64	>64	>64	>64	64
7c	0.19	>64	>64	>64	>64	>64	64
7g	0.28	>64	>64	>64	>64	>64	>64
7h	0.33	>64	>64	>64	>64	>64	>64
7i	0.68	>64	>64	>64	>64	>64	>64
7j	0.90	>64	>64	>64	>64	>64	>64
15a	0.21	>64	>64	>64	>64	>64	>64
15b	0.60	>64	>64	>64	>64	>64	>64
15d	1.67	>64	>64	>64	>64	>64	32
15e	3.19	>64	>64	>64	>64	>64	>64
Isoniazid	ND	0.03	0.03	0.03	0.03	0.03	0.06

^{a} D7 and D14, incubation for 7 and 14 days, respectively, at 37°C; ND, not done.

group at the 3′ position (24p) in our model would cause a close contact to the ring of Tyr177 but may be better accommodated by flipping the pyridine ring. The introduction of groups at the 2′ position (24r and 24s) would cause intramolecular close contacts. Changing the aza position to 4′-pyridyl (24d and 24q) produces a 100-fold loss of potency. The HB interactions differ at the acid/amide group substitution but have a minimal effect on potency. In the case of 24j, the carboxylate group makes direct HB interactions with side chains of Tyr182. In the 25b complex, the interaction with Arg238 is absent. The side chains of Asn277 and Tyr235, which are important for triazole binding, make only solvent-mediated hydrogen bonds with the biaryls.

Comparison of the triazole and biaryl binding modes. The triazole and biaryl compounds occupy similar binding sites (Fig. 5D). The thioether and alkylamide side chains of the triazole scaffold overlap the ether and aryl-piperazine side chains of the biaryl scaffold, respectively. The triazole extensions are longer and extend closer to the ATP binding site. The potential contact with the gamma-phosphate of ATP may explain why the triazoles are competitive ATP inhibitors whereas the biaryl compounds are not. The substituted benzyl group extending from the triazole core overlaps the para-nitrilephenyl group of biaryls. Although both compound classes form extensive networks of hydrogen bond interactions, no PanK partner forms a hydrogen bond with both inhibitors. A structurally conserved water molecule, however, makes a HB interaction with either the pyridine of the biaryls or the carbonyl oxygen of the amide linker of the triazoles.

Target vulnerability studies. (i) *In vitro* vulnerability of *Mt*PanK. Despite having nanomolar potency on the enzyme, the triazole class did not yield MICs for the wild-type *M. tuberculosis* H37Rv strain, whereas the biaryls had MICs, although they were severalfold higher than the IC$_{50}$. This prompted us to investigate the vulnerability of PanK both *in vitro* and *in vivo* using a *Mt*PanK knockdown strain.

M. tuberculosis possesses two isoforms of pantothenate kinase encoded by the *coaA* and *coaX* genes. While there is essentiality information available for both, *coaX* has been shown to be nonessential for the survival of *M. tuberculosis* in macrophages and in

animals (9). However, there are no reports on the vulnerability of *Mt*PanK to indicate the extent to which its levels need to be reduced to achieve bacterial growth inhibition.

A *M. tuberculosis coaA* conditional-expression strain was generated in which the *coaA* expression is regulated by the pristinamycin-inducible promoter. A set of PCRs confirmed the genotype of the recombinant strain, i.e., the presence of a hygromycin selection marker and the presence of a full-length *coaA* gene downstream of the pPTR promoter and the truncated gene downstream of the wild-type promoter (data not shown).

The minimum inducer concentration required to support growth of *M. tuberculosis coaA*KD was determined by plating for survivors on 7H10 media supplemented with 0, 2, 10, 25, 50, and 100 ng/ml of P$_1$. While the growth of *M. tuberculosis* H37Rv culture remained unaffected at these concentrations of P$_1$ (data not shown), the *M. tuberculosis coaA*KD strain could not grow on agar plates unless supplemented with at least 10 ng/ml of P$_1$ (Fig. 6), thus confirming its essentiality *in vitro*. In order to understand the vulnerability of *Mt*PanK, a time-to-death study combined with intracellular target level measurements was performed. Viability was monitored through measurements of A_{600} and CFU (on agar plates with 10 ng/ml P$_1$) at regular intervals for up to 15 days. Surprisingly, the *M. tuberculosis coaA*KD culture grew well in liquid cultures even in the absence of P$_1$ (Fig. 7A). This was in contrast to our earlier observation, wherein no survivors could be isolated in the absence of P$_1$ on solid media. This growth trend continued until the end of day 15, when all cultures were terminated due to appearance of clumps. This observation suggested that within the approximately 15 generations that the *coaA*KD culture went through in the absence of inducer, the PanK was not titrated down to levels incompatible with growth. In order to substantiate this hypothesis, the *coaA*KD culture was subjected to dilutions in fresh media and incubated further to provide more generations, which would help in reducing the protein levels. However, these experiments were not conclusive owing to clumping of cultures within 48 h of dilution. Leaky expression of *Mt*PanK from the inducible promoter was ruled out by Western blotting of the culture samples (Fig. 7B). While hardly any *Mt*PanK could be detected in culture without P$_1$, the *M. tuberculosis* sigma 70 (*Mt*SigA) internal control could be detected to the same levels as seen with wild-type *M. tuberculosis* H37Rv (Fig. 7B). The results detailed above suggest that *Mt*PanK is not a vulnerable target *in vitro*, as even a very small amount of the enzyme seemed to be sufficient for bacterial growth.
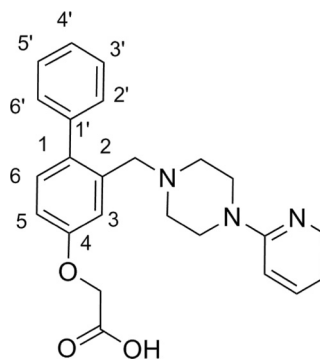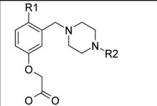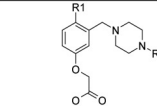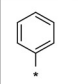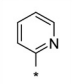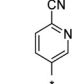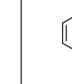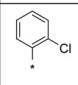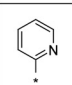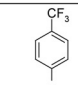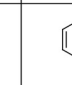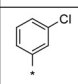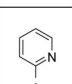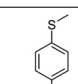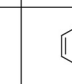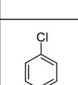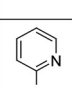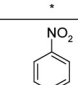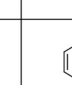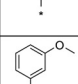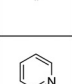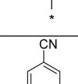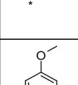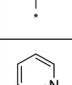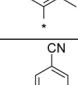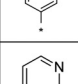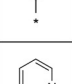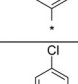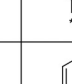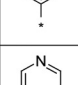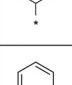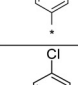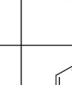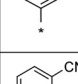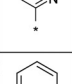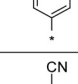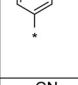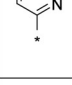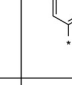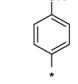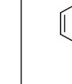

FIG 4 Generic structure of biaryl acetic acid.

TABLE 5 Illustration of SAR of biaryl acetic acids

Entry	R1	R2	IC$_{50}$ (µM)	MIC (µg/ml)	Entry	R1	R2	IC$_{50}$ (µM)	MIC (µg/ml)
24a	phenyl	2-pyridyl	9.2	32	24k	2-cyanopyridyl	2-pyridyl	0.2	32
24b	2-Cl-phenyl	2-pyridyl	3.5	32	24l	4-CF$_3$-phenyl	2-pyridyl	0.7	32
24c	3-Cl-phenyl	2-pyridyl	3.9	32	24m	4-SMe-phenyl	2-pyridyl	0.6	64
24d	4-Cl-phenyl	2-pyridyl	0.24	64	24n	4-NO$_2$-phenyl	2-pyridyl	0.07	32
24e	3-OMe-phenyl	2-pyridyl	4.8	32	24o	4-CN-3-Me-phenyl	2-pyridyl	0.02	32
24f	4-OMe-phenyl	2-pyridyl	1.2	32	24p	4-CN-phenyl	6-Me-pyridyl	0.36	64
24g	3-pyridyl	2-pyridyl	6.7	32	24q	4-Cl-phenyl	4-pyridyl	22	32
24h	4-pyridyl	2-pyridyl	9.2	32	24r	4-Cl-phenyl	2-OMe-phenyl	50	32
24i	3-CN-phenyl	2-pyridyl	7.8	32	24s	4-CN-phenyl	2-CN-phenyl	50	32
24j[a]	4-CN-phenyl	2-pyridyl	0.2	32	24t[a]	4-CN-phenyl	2-pyridyl	50	32
[a] Entries 24j and 24t are similar in terms of R1 and R2. However, an extra Me group has been introduced into the side chain of 24t next to piperazine.					24u	4-OMe-phenyl	6-Me-pyridyl	0.45	>64

(ii) *In vivo* essentiality of *Mt*PanK. The phenotype of *coaA*KD *M. tuberculosis* strain in mice was studied in parallel with that of the *M. tuberculosis* H37Rv wild-type strain. BALB/c mice were infected via the intravenous route with the *M. tuberculosis* H37Rv strain or the *M. tuberculosis coaA*KD strain grown in the presence of 10 ng/ml P$_1$. Owing to the poor pharmacokinetic properties of P$_1$ in mice (unpublished data), the course of infection had to be monitored under inducer-depleted conditions only. The bacterial burdens in lungs and spleen of infected mice were monitored over 150 days on plates supplemented with 50 ng/ml of P$_1$. At the end of the 150-day study, the *coaA*KD strain exhibited a very small dif-ference in the growth rate compared to that o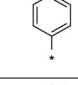f the control *M. tuberculosis* H37Rv strain, albeit at a statistically insignificant level (Fig. 7C), suggesting poor vulnerability of *Mt*PanK *in vivo* as well.

(iii) *In silico*-based vulnerability test of *Mt*PanK. In this study, chemical vulnerability of *Mt*PanK was modeled and evaluated using the *in silico M. tuberculosis* platform. This model has the unique capability of predicting both the differential levels of effectiveness among the three types of inhibition (competitive, uncompetitive, and noncompetitive) (16, 18) and the ensuing growth inhibition. Towards this goal, PanK inhibition and the resultant flux following different types of inhibition were simulated in the

TABLE 6 SAR at the aryloxyacetic acid position of compound 8

Entry	R1	R2	IC$_{50}$ (μM)	MIC (μg/ml)	Entry	R1	R2	IC$_{50}$ (μM)	MIC (μg/ml)
25a	4-CN phenyl	H$_2$N–C(O)–CH$_2$–	0.21	64	22b[a]	4-CN phenyl	EtO–C(O)–CH$_2$–	50	4
25b	4-CN phenyl	CH$_3$HN–C(O)–CH$_2$–	0.55	64	21b	3-Cl phenyl	MeO–C(O)–CH$_2$–	5	8
21a	4-CN phenyl	MeO–C(O)–CH$_2$–	0.89	4	21c	3-OMe phenyl	MeO–C(O)–CH$_2$–	12.5	8
22a	4-CN phenyl	EtO–C(O)–CH$_2$–	0.97	4	22c	2-Cl phenyl	EtO–C(O)–CH$_2$–	21	8
23a	4-OMe phenyl	t-BuO–C(O)–CH$_2$–	>50	16	21d	3-CN phenyl	MeO–C(O)–CH$_2$–	21	32
23b[a]	4-OMe phenyl	t-BuO–C(O)–CH$_2$–	>50	16	26	4-CN phenyl	tetrazolyl–CH$_2$–	0.41	64
23c	4-Cl phenyl	t-BuO–C(O)–CH$_2$–	>50	16					

[a]Entries 22b and 23b have the following side chain [N-ethyl piperazine linked to 6-methylpyridin-2-yl]

platform and the [I]/K_i ratio was deduced with the aim of ranking them based on analysis of the type which yields early growth arrest. However, in order to simulate various kinds of inhibitions of the reaction, it was important to know the *M. tuberculosis* PanK reaction mechanism. In *M. tuberculosis*, PanK catalyzes a bisubstrate reaction, the two substrates being pantothenate and ATP. In the absence of any clear verification of the mode of the actual reaction mechanism for PanK in *M. tuberculosis*, the mechanism simulated in the *in silico* platform was as reported earlier for *E. coli* (16) wherein this enzyme follows a sequential mechanism, with

ATP binding first and pantothenate next (19). Within the various classes of inhibitors, in mixed-mode inhibition the inhibitor binds sequentially to the free enzyme and to the enzyme-substrate complex. Therefore, in this mode of inhibition, the inhibitor, when modeled in the platform, is both competitive and uncompetitive with ATP. Since such an inhibitor binds both forms of the enzyme, it could be more potent than those which target only one form of the enzyme.

In the current study, following simulation, the predicted [I]/K_i ratios that were required to reduce the CoA pathway flux to below
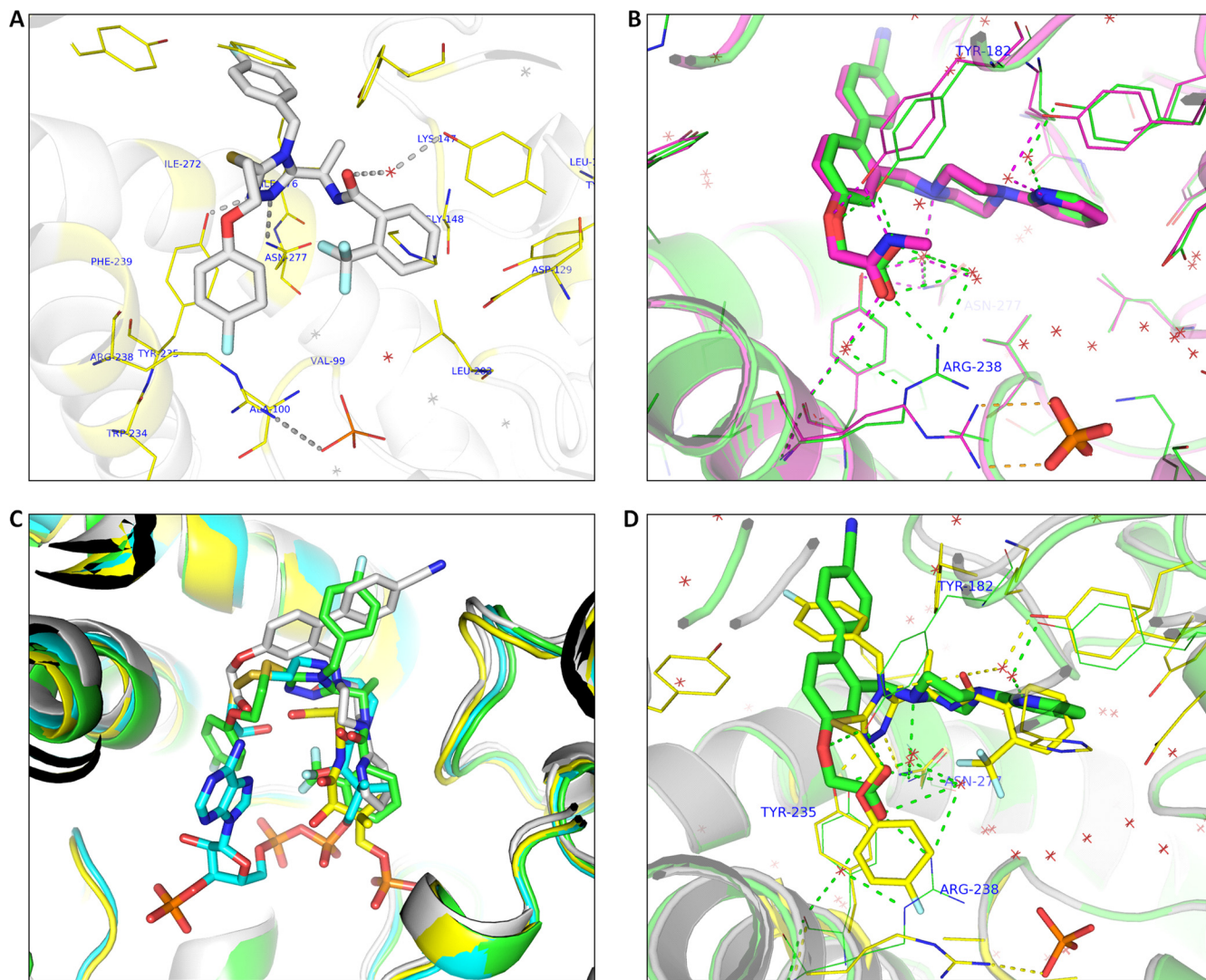
FIG 5 (A) The typical binding mode of triazole class is represented by compound 7i (gray carbons) in the *Mt*PanK active site (PDB ID 4BFW). Key residues (as lines) involved in the interactions are shown in yellow. (B) Showing the typical binding mode of the biaryl class exemplified by compound 24j (green carbons) and compound 25b (pink carbons) representing acid and amide functionality at ether linkage, respectively, in the *Mt*PanK active site (PDB ID 4BFY and 4BFZ). Key residues (as lines) involved in the interactions are also shown in the respective ligand carbon colors. In the case of the amide structure, Arg238 has a different rotamer, whereas Tyr182 has shown a tendency of having two different rotamers. (C) Superposition of the active site of *Mt*PanK crystal structures showing triazole compound 7i (green), biaryl compound 24j (gray), phosphopantothenate (yellow, PDB ID 2ZSA), and CoA (cyan, PDB ID 2GES). (D) Superposition of triazole as represented by compound 7i (yellow carbons, PDB ID 4BFW) and biaryl as represented by compound 24j (green carbons, PDB ID 4BFY) in the *Mt*PanK active site. The active-site residues (as lines) are also shown in the respective ligand carbon colors.

a critical value of 0.07 µmol/s (equivalent to the MIC) were found to be 80, 12, 400, and 10,000 µM for competitive, mixed, noncompetitive, and uncompetitive modes of inhibition, respectively. These observations demonstrated that mixed inhibition would be the preferred mode that would require the lowest inhibitor concentration for an early biomass arrest (Fig. 8).

DISCUSSION

Although the essentiality of a gene is considered to be one of the key attributes for choosing an antibacterial target, chemical moieties against vulnerable targets are preferable in an anti-infective discovery program. Vulnerability is defined as the extent of inhibition of a target required to have a negative impact on growth, leading to cell death (20). As this parameter varies
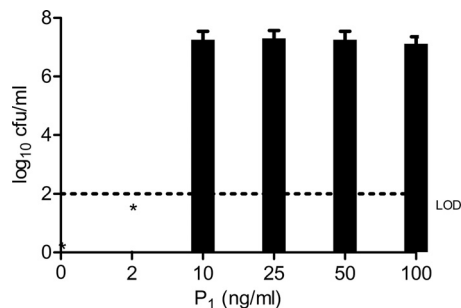

FIG 6 Dependence of the *M. tuberculosis coaA*KD strain on P_1. The conditional-expression strain was grown with 100 ng/ml of P_1 until mid-log phase. Washed cells were diluted in fresh medium and plated on 7H10 plates supplemented with different concentrations of P_1. Data are representative of the results of 3 independent experiments. LOD, limit of detection; *, below the LOD.
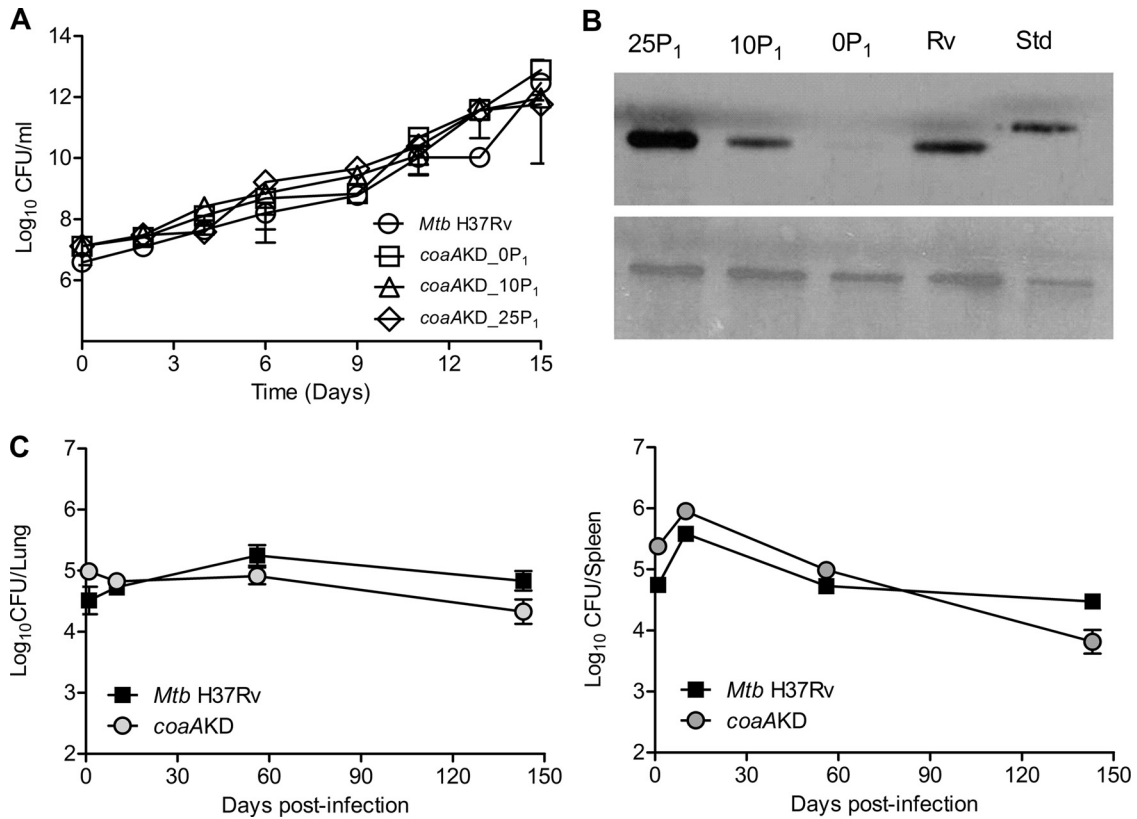
FIG 7 (A) Growth kinetics of *M. tuberculosis coaA*KD strain. A growth kinetics study was performed to assess the time required to achieve a bactericidal effect in the absence of inducer P_1. The *M. tuberculosis coaA*KD strain was grown with 10 ng/ml of P_1 until an A_{600} of ~0.2 was reached. Harvested and washed cells were used to inoculate cultures supplemented with 0, 10, or 25 ng/ml of P_1. Culture growth was monitored by plating for survivors on plates containing P_1. The data are a representation of the results of two such experiments. (B) Effect of P_1 concentration on *Mt*PanK expression in the *M. tuberculosis coaA*KD strain. Protein samples prepared from day 6 postexposure to P_1 of the growth kinetics study were used for Western blot analyses. Two micrograms of total protein from the lysates were loaded per lane, blotted, and probed with anti-*Mt*PanK antibody (top panel) or *Mt*SigA antibody (bottom panel). $0P_1$, $10P_1$, and $25P_1$ represent the P_1 concentrations (in ng/ml) used in the growth kinetics study. Rv data represent a sample from the *M. tuberculosis* H37Rv control. Std data represent $His_{(6)}$-PanK in the top panel and $His_{(6)}$-SigA in the bottom panel. (C) *In vivo* phenotype of *M. tuberculosis coaA*KD strain. Mice were infected by the intravenous (i.v.) route with the *M. tuberculosis* H37Rv strain and *M. tuberculosis coaA*KD strain with 3 mice per time point. The course of infection was monitored over 150 days postinfection in the absence of P_1 supplementation. Bacterial loads in lungs and spleen were measured by plating organ homogenates for CFU on 7H10 plates for the control strain and 7H10 plates supplemented with 50 ng/ml of P_1 for the conditional-expression strain.

from one target to another, the best target would be the one that requires minimal perturbation to kill the pathogen, whereas nonvulnerable targets may require more than 90% inhibition to adversely affect growth (21–23). In order to assess

the vulnerability of a target in *M. tuberculosis*, one would have to monitor growth inhibition by either using compounds with different modes of inhibition against the target or gradually reducing the levels of target gene expression in the bacterial cell. However,
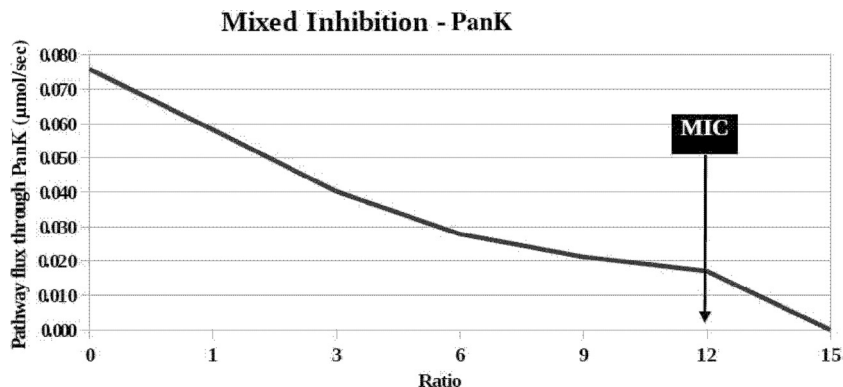

FIG 8 Mixed mode of inhibition of *Mt*PanK and the resultant flux through the pathway. The predicted $[I]/K_i$ ratio required to reduce the CoA pathway flux to below a critical value of 0.07 μmol/s (indicated as the MIC) was the least for the mixed mode of inhibition (11).

the latter is reflective of only one type of chemical inhibition and hence is not appropriate for direct extrapolation of the effect of one to estimate the effect of the other. Additionally, a chemical inhibitor could bring in effects that are more pleiotropic (12, 23), whereas a genetic knockdown is very specific to the intended target. An *in silico* platform would enable prediction of the extent of target depletion or the type of inhibitor needed to evaluate novel targets whose vulnerability is not understood. From the simulation profiles observed, it was evident that for *Mt*PanK, a mixed mode of inhibition would most likely result in growth inhibition at a much lower inhibitor concentration.

In the present study, *Mt*PanK, an essential bacterial enzyme, was extensively evaluated as a putative target for the discovery of novel antituberculosis drugs. Results reported here indicate that targets such as *Mt*PanK are amenable to a range of biochemical and biophysical studies, thus offering opportunities to invest in HTS to identify inhibitors with maximum structural and mechanistic diversity, ATP competitive and ATP noncompetitive, which could possibly serve as start points for a lead identification program(s). PanK inhibition within *M. tuberculosis* through the use of ATP competitors (triazoles) may require very high potency to inhibit the enzyme inside the cell, since the intracellular ATP concentration of around 1 mM (24) is in 10-fold excess of its K_m for ATP. Per the Cheng-Prusoff relationship (25) between IC_{50} and K_i, a competitive inhibitor may require a much (>10-fold) higher concentration to achieve the same degree of inhibition, as obtained by a noncompetitive or uncompetitive inhibitor with an equivalent K_i value. Hence, IC_{50}s were determined at 50× K_m of ATP to closely mimic the physiological condition inside the cell.

In the case of triazoles and quinolones, even with potencies of about 100 nM and 200 nM, respectively, at 50× K_m of ATP, cellular inhibition could not be achieved. These results suggested that either a more potent competitive inhibitor or an inhibitor with a different mode of inhibition is required. However, these inhibitors demonstrated growth inhibition of *M. tuberculosis* in cells with reduced *Mt*PanK levels (*coaA*KD) along similar lines as reported earlier for another target from the same pathway (31). These data clearly indicate that with lowered expression levels, the inhibitor is able to engage the target and bring about *M. tuberculosis* growth inhibition, suggesting that *Mt*PanK is poorly or weakly vulnerable. The observations reported here match earlier reports in *E. coli* (26–28), where it was shown that an adverse effect on bacterial growth required >95% enzyme inhibition against a few enzymes of the CoA biosynthetic pathway, sustained over several generations.

Since ATP-competitive inhibitors did not demonstrate cellular activity against wild-type *M. tuberculosis*, as an alternative, the mixed noncompetitive inhibitors (modified biaryl acids) were also evaluated and optimized for lead identification. While the original hits inhibited the enzyme at a micromolar concentration, the IC_{50} could be improved to 22 nM by systematic changes. True binding of these compounds was confirmed by midpoint (T_m) shift experiments followed by elucidation of cocrystal structures with inhibitors of both triazole and biaryl classes (11). The crystal structures not only gave information about key residues for binding of both classes of inhibitors but also hinted at the observed difference in the modes of inhibition. Free carboxylic acids with potent IC_{50}s failed to show cellular activity, indicating the inability to permeate the *M. tuberculosis* cell wall. However, biaryl acetic

acid derivatives (esters) with $IC_{50} < 1$ μM had *M. tuberculosis* MICs ranging between 4 and 16 μg/ml. The mode of action of a few of these active esters was confirmed by the reduced cellular activity against *M. bovis* BCG overexpressing *Mt*PanK (MIC > 64 μg/ml). This observation helped to link the enzyme inhibition with the MIC and thus provided an additional proof of the chemical validation of PanK as a possible drug target in *M. tuberculosis*.

All classes of *Mt*PanK inhibitors discussed in this report could be optimized to nanomolar potencies regardless of their mode of inhibition ($IC_{50} \leq 50$ nM when both substrates for *Mt*PanK were maintained at K_m). However, only inhibitors that did not have a competitive mechanism of inhibition had antimycobacterial activity. This differential response was earlier demonstrated using *in silico*-based simulation studies in *E. coli* (16). In that report, for *Mt*PanK, $[I]/K_i$ was lowest with mixed noncompetitive inhibitors. Growth inhibition in the presence of a mixed noncompetitive inhibitor was preceded by a steady decline in PanK levels to below the critical level of 5% (16). Cross-species applicability of this *E. coli* platform was tested and confirmed by comparing predictions with the experimental data generated using a mycobacterial species (16). Since both the triazoles and the biaryl esters showed modulation of MICs in *M. tuberculosis* strains expressing different levels of PanK, a direct and specific link to target could be established.

Unlike targets that are involved in essential housekeeping processes, for targets such as PanK, for which there is no clinical precedent, an evaluation of their vulnerability is necessary. To this end, a parallel effort involving evaluation of *M. tuberculosis coaA*KD with regard to its growth kinetics *in vitro* and *in vivo* was carried out. In all of these experiments, the survivors were checked on 7H10 plates with P₁ and, for revertants, without P₁.

The *M. tuberculosis coaA*KD strain demonstrated complete inducer dependence for growth on solid agar medium, thereby establishing its essentiality. The *in vitro* survival kinetic studies in the absence of inducer indicated growth rates similar to those of wild-type strains as observed by CFU recovered from the plates with P₁. In the case of *in vivo* phenotyping experiments, however, small differences in growth rates were seen, albeit the differences was insignificant. This observation suggested either that the *M. tuberculosis coaA*KD strain had reverted through accumulation of genetic mutation or that there was leaky expression of *Mt*PanK. The possibility of strain reversion was ruled out, as the very same samples failed to grow on 7H10 plates without P₁. With regard to the leaky expression, *Mt*PanK could not be detected on day 6 postwithdrawal of inducer in Western blots. However, the recovery of viable cells from broth could be attributed to the presence of trace amounts of *Mt*PanK undetectable by Western blots. If such low levels of *Mt*PanK can keep the cells viable, the current studies indicate that a nearly 100% depletion of the target is required to achieve growth inhibition. As *M. tuberculosis* is known to have a long generation time, a single cell may need to go through nearly 30 generations to form a visible colony on solid medium, enough for CoA to drop below critical levels.

According to earlier reports, a reduction in PanK activity of more than 95% was required to achieve growth inhibition since the steady-state levels of CoA are far in excess of what is critical for cell survival (24, 27, 28). Results from the current study are in concurrence with these earlier observations and were further substantiated by the inability to recover colonies on solid me-

dium. However, the broth experiments could be conducted only for a maximum of 15 days (for reasons of cell clumping), during which the PanK levels may not have become depleted below critical levels. In addition, under conditions where the strain exists in a nearly nonreplicating phase in an animal model, reduction in CoA levels could be very minimal and hence would explain the recovery of *M. tuberculosis* even after long periods *in vivo*. The vulnerability studies, both genetic and chemical, reported here demonstrate that PanK is not an attractive antimycobacterial target. This is similar to the data observed in earlier studies with a Δ*panCD M. tuberculosis* strain (29), wherein the auxotrophic mutant persisted in the lungs and spleens of infected mice for over 6 months following intravenous infection. Since PanCD and PanK are both enzymes from the CoA biosynthetic pathway, the observations from this study and the earlier Δ*panCD* report suggest the possible poor vulnerability of targets of this pathway.

The results described here have thus unraveled the importance of understanding the vulnerability of a novel target either through the use of conditional-expression strains and/or via inhibitors with diverse mechanistic activities before embarking on a drug discovery program.

ACKNOWLEDGMENTS

REFERENCES

1. **WHO.** 2012. Global tuberculosis report WHO. World Health Organization, Geneva, Switzerland.
2. **Raviglione M, Marais B, Lönnroth FK, Getahun H, Migliori GB, Harries AD, Nunn P, Lienhardt C, Graham S, Chakaya J, Weyer K, Cole S, Kaufmann SH, Zumla A.** 2012. Scaling up interventions to achieve global tuberculosis control: progress and new developments. Lancet **379:**1902–1913. http://dx.doi.org/10.1016/S0140-6736(12)60727-2.
3. **Lönnroth K, Jaramillo E, Williams BG, Dye C, Raviglione M.** 2009. Drivers of tuberculosis epidemics: the role of risk factors and social determinants. Soc. Sci. Med. **68:**2240–2246. http://dx.doi.org/10.1016/j.socscimed.2009.03.041.
4. **Zumla A, Abubakar I, Raviglione M, Hoelscher M, Ditiu L, Mchugh TD, Squire SB, Cox H, Ford N, McNerney R, Marais B, Grobusch M, Lawn SD, Migliori GB, Mwaba P, O'Grady J, Pletschette M, Ramsay A, Chakaya J, Schito M, Swaminathan S, Memish Z, Maeurer M, Rifat Atun R.** 2012. Drug-resistant tuberculosis - current dilemmas, unanswered questions, challenges, and priority needs. J. Infect. Dis. **205:**S228–S240. http://dx.doi.org/10.1093/infdis/jir858.
5. **Spry C, Kirk K, Saliba KJ.** 2008. Coenzyme biosynthesis, an antibacterial drug target. FEMS Microbiol. Rev. **32:**56–106. http://dx.doi.org/10.1111/j.1574-6976.2007.00093.x.
6. **Martinelli LK, Aldrich CC.** 2012. Antimetabolite poisoning of cofactor biosynthesis. Chem. Biol. **19:**543–544. http://dx.doi.org/10.1016/j.chembiol.2012.05.004.
7. **Gerdes SY, Scholle MD, D'Souza M, Bernal A, Baev MV, Farrell M, Kurnasov OV, Daugherty MD, Mseeh F, Polanuyer BM, Campbell JW, Anantha S, Shatalin KY, Chowdhury SA, Fonstein MY, Osterman AL.** 2002. From genetic footprinting to antimicrobial drug targets: examples in cofactor biosynthetic pathways. J. Bacteriol. **184:**4555–4572. http://dx.doi.org/10.1128/JB.184.16.4555-4572.2002.
8. **Vallari DS, Jackowski S, Rock CO.** 1987. Regulation of pantothenate kinase by coenzyme A and its thioesters. J. Biol. Chem. **262:**2468–2471.
9. **Awasthy D, Ambady A, Bhat J, Sheikh G, Ravishankar S, Subbulakshmi V, Mukherjee K, Sambandamurthy V, Sharma UK.** 2010. Essentiality and functional analysis of type I and type III pantothenate kinases of *Mycobacterium tuberculosis.* Microbiology **156:**2691–2701. http://dx.doi.org/10.1099/mic.0.040717-0.
10. **Venkatraman J, Bhat J, Solapure SM, Sandesh J, Sarkar D, Aishwarya S, Mukherjee K, Datta S, Malolanarasimhan K, Bandodkar B, Das K.** 2012. Identification and characterization of mechanistically diverse inhibitors of the mycobacterial tuberculosis enzyme, pantothenate kinase [CoaA]. J. Biomol. Screen. **17:**293–302. http://dx.doi.org/10.1177/1087057111423069.
11. **Björkelid C, Bergfors T, Raichurkar AK, Mukherjee K, Malolanarasimhan K, Bandodkar B, Jones TA.** 2013. Structural and biochemical characterization of compounds inhibiting *Mycobacterium tuberculosis* PanK. J. Biol. Chem. **288:**18260–18270. http://dx.doi.org/10.1074/jbc.M113.476473.
12. **Kaur P, Agarwal S, Datta S.** 2009. Delineating bacteriostatic and bactericidal targets in Mycobacteria using IPTG inducible antisense expression. PLoS One **4:**e5923. http://dx.doi.org/10.1371/journal.pone.0005923.
13. **Forti F, Costa A, Ghisotti D.** 2009. Pristinamycin inducible gene regulation in mycobacteria. J. Biotechnol. **140:**270–277. http://dx.doi.org/10.1016/j.jbiotec.2009.02.001.
14. **Clinical and Laboratory Standards Institute (CLSI).** 2011. Susceptibility testing of mycobacteria, nocardiae, and other aerobic actinomycetes; approved standard—2nd ed. CLSI, Wayne, PA.
15. **Collins L, Franzblau SG.** 1997. Microplate alamar blue assay versus BACTEC 460 system for high-throughput screening of compounds against *Mycobacterium tuberculosis* and *Mycobacterium avium.* Antimicrob. Agents Chemother. **41:**1004–1009.
16. **Barve A, Gupta A, Solapure SM, Kumar A, Ramachandran V, Seshadri K, Vali S, Datta S.** 2010. A kinetic platform for in silico modelling of the metabolic dynamics in *Escherichia coli.* Adv. Appl. Bioinform. Chem. **2010:**1–14. http://dx.doi.org/10.2147/AABC.S14368.
17. **Yun M, Park CG, Kim JY, Rock CO, Jackowski S, Park HW.** 2000. Structural basis for the feedback regulation of *Escherichia coli* pantothenate kinase by coenzyme A. J. Biol. Chem. **275:**28093–28099.
18. **Ramachandran V, Singh R, Yang X, Tunduguru R, Mohapatra S, Khandelwal S, Patel S, Datta S.** 2013. Genetic and chemical knockdown: a complementary strategy for evaluating an anti-infective target. Adv. Appl. Bioinform. Chem. **6:**1–13. http://dx.doi.org/10.2147/AABC.S39198.
19. **Song WJ, Jackowski S.** 1994. Kinetics and regulation of pantothenate kinase from *Escherichia coli.* J. Biol. Chem. **269:**27051–27056.
20. **Datta S.** 1999. Understanding the characteristics of a good anti-infective drug target. J. Parasit. Dis. **23:**139–140.
21. **Kohanski MA, Dwyer DJ, Hayete B, Lawrence CA, Collins JJ.** 2007. A common mechanism of cellular death induced by bactericidal antibiotics. Cell **130:**797–810. http://dx.doi.org/10.1016/j.cell.2007.06.049.
22. **Jørgensen CM, Hammer K, Jensen PR, Martinussen J.** 2004. Expression of the pyrG gene determines the pool sizes of CTP and dCTP in *Lactococcus lactis.* Eur. J. Biochem. **271:**2438–2445. http://dx.doi.org/10.1111/j.1432-1033.2004.04168.x.
23. **Wei J, Krishnamoorthy V, Murphy K, Kim J, Schnappinger D, Alberd T, Sassetti CM, Rhee KY, Rubin EJ.** 2011. Depletion of antibiotic targets has widely varying effects on growth. Proc. Natl. Acad. Sci. U. S. A. **108:**4176–4181. http://dx.doi.org/10.1073/pnas.1018301108.
24. **Buchholz A, Takors R, Wandrey C.** 2001. Quantification of intracellular metabolites in *Escherichia coli* K12 using liquid chromatographic-electrospray ionization tandem mass spectrometric techniques. Anal. Biochem. **295:**129–137. http://dx.doi.org/10.1006/abio.2001.5183.
25. **Cheng Y, Prusoff WH.** 1973. Relationship between the inhibition constant (KI) and the concentration of inhibitor which causes 50 per cent inhibition (I50) of an enzymatic reaction. Biochem. Pharmacol. **22:**3099–3108. http://dx.doi.org/10.1016/0006-2952(73)90196-2.
26. **Song WJ, Jackowski S.** 1992. Cloning, sequencing, and expression of the pantothenate kinase (coaA) gene of *Escherichia coli.* J. Bacteriol. **174:**6411–6417.
27. **Zhang YM, Frank MW, Virga KG, Lee RE, Rock CO.** 2004. Acyl carrier protein is a cellular target for the antibacterial action of the pantothenamide class of pantothenate antimetabolites. J. Biol. Chem. **279:**50969–50975. http://dx.doi.org/10.1074/jbc.M409607200.
28. **Christopherson RI, Duggleby RG.** 1983. Metabolic resistance: the protection of enzymes against drugs which are tight-binding inhibitors by the

accumulation of substrate. Eur. J. Biochem. **134:**331–335. http://dx.doi .org/10.1111/j.1432-1033.1983.tb07571.x.

29. **Sambandamurthy VK, Derrick SC, Jalapathy KV, Chen B, Russell RG, Morris SL, Jacobs WR, Jr.** 2005. Long-term protection against tuberculosis following vaccination with a severely attenuated double lysine and pantothenate auxotroph of *Mycobacterium tuberculosis.* Infect. Immun. **73:**1196–1203. http://dx.doi.org/10.1128/IAI.73.2.1196 -1203.2005.

30. **Leonardi R, Zhang YM, Charles OR, Jackowski S.** 2005. Coenzyme A: back in action. Prog. Lipid Res. **44:**125–153. http://dx.doi.org/10.1016/j .plipres.2005.04.001.

31. **Abrahams GL, Kumar A, Savvi S, Hung AW, Wen S, Abell C, Barry CE, III, Sherman DR, Boshoff HI, Mizrahi V.** 2012. Pathway-selective sensitization of *Mycobacterium tuberculosis* for target-based whole-cell screening. Chem. Biol. **19:**844–854. http://dx.doi.org/10.1016/j.chembiol .2012.05.020.